On the sensitivity of a laser heterodyne polarimeter for vacuum birefringence detection

Gabriel Alberts[1], Hal Hollis[1], Harrison LaBollita[2], Guido Mueller[1]

[1]Department of Physics, University of Florida, Gainesville, FL, 32611
[2]Department of Mathematics and Physics, Piedmont College, Demorest, GA, 30535

Detecting vacuum magnetic birefringence (VMB) requires an immensely accurate, precisely calibrated experiment. We are working on a new design to detect the birefringence (BF) of individual optical components without a cavity that can also be used to measure VMB in reflection off a cavity. Our design uses two overlapping, orthogonally polarized laser beams to measure the relative phase difference between a reference path and one with rotating polarizations, which may experience oscillating phase shifts in vacuum in the presence of a magnetic field. To test the design, we developed a small-scale setup without cavities that can analyze different birefringent sources with the same principle. Our early results from testing mirrors show spatial variations in BF due to imperfect mirror coatings and show no correlation between the strength of a magnetic field applied parallel to the mirror's surface and BF amplitude. In addition to assisting in the selection of suitable components for the final design, our laser heterodyne polarimeter (LHP) promises more sensitive results than previous experiments and may very well be the basis for the very first detection of VMB.

INTRODUCTION

The classical vacuum is a region of space devoid of matter and any physical fields that carry energy and momentum. This "free space" is therefore the lowest possible energy state of a classical system and has zero energy. It also acts the reference state for the permittivity of a material making its relative permittivity identically one. This vacuum does not influence matter in any way and therefore acts only as a medium for gravitational and electromagnetic waves to propagate. The quantum vacuum, on the other hand, is the quantum state with the lowest possible energy, which is nonzero due to vacuum fluctuations. These fluctuations can be attributed to the creation and annihilation of virtual particle-antiparticle pairs that temporarily disturb the vacuum's energy.

In quantum electrodynamics (QED), a more particular QED vacuum is needed to fit the theory. This vacuum again describes a lowest possible energy state but now it is of the electromagnetic field when both the electric and magnetic fields are quantized. The quantization of these fields then gives the QED vacuum a relative permittivity that is not one, as is the case for the classical vacuum. Since the propagation of an electromagnetic wave is influenced by this value, the QED vacuum is capable of exhibiting birefringent effects. Birefringence is an optical property of a material with a polarization-dependent index of refraction.

VMB was first mentioned formally by Dirac in 1934 during the early development of QED. In a paper on the theory of the positron, or antielectron, Dirac states:

> Further work that remains to be done is to examine the physical consequences of the foregoing assumptions and to see whether it leads to any phenomena of the nature of a polarization of a vacuum by an electromagnetic field.[1]

Just months after, Heisenberg published his "Remarks on Dirac's theory of the positron," which included a discussion on this postulate.[2] With these two papers at hand, many theorists began contributing to the theory with Serber[3] and Uehling[4] expanding Maxwell's field equations and Coulomb's law respectively to account for the effect. In 1936, Heisenberg and Euler derived the Euler-Heisenberg Lagrangian,[5] which established a foundation to analytically solve for the effects of VMB. Considering one loop contributions, this can be presented in the weak field limit and for slowly varying electromagnetic fields as

$$\mathcal{L} = \frac{1}{2\mu_0}\left(\frac{\mathrm{E}^2}{c^2} - B^2\right) + \frac{A_e}{\mu_0}\left[\left(\frac{E^2}{c^2} - B^2\right)^2 + 7\left(\frac{\mathbf{E}}{c}\cdot\mathbf{B}\right)^2\right] \quad (1)$$

where

$$A_e = \frac{\alpha^2\lambda_e^3}{180\mu_0\pi^3 m_e c^2} = 1.32\times10^{-24}\ \mathrm{T}^{-2} \quad (2)$$

with $\lambda_e = h/(m_e c)$ being the Compton wavelength of the electron, $\alpha = e^2/(4\pi\varepsilon_0\hbar c)$ the fine structure constant, and m_e the mass of the electron. Karplus and Neuman showed[6] that for complex indices of refraction, VMB can be expressed

$$\Delta n = n_{\parallel} - n_{\perp} = 3A_e B^2 \quad . \quad (3)$$

While multiple astronomical observations are currently being pursued to account for these effects, we are interested in the direct observation of VMB. Several

projects in the past have shared this objective but none have been able to detect the effect with enough sensitivity and confidence. Experiments conducted at CERN[7] and Brookhaven National Laboratory[8] as well as Legnaro and Ferrara as part of the PVLAS collaboration[9] utilized high-finesse cavities and found either a signal was not detected at the expected sensitivity using a given magnetic field strength, or that the time needed to reach a particular heightened sensitivity was unreasonably long. We believe that performing a modified experiment to the one originally published by Hall, Ye, and Ma[10] using advanced gravitational wave detection technology from LIGO and LISA in the ALPS IIc design will give us the sensitivity necessary to measure VMB.

While the ALPS (Any Light Particle Search) experiment was founded to search for WISPs (very Weakly Interacting Sub-eV Particles), its facility can serve multiple purposes. The general design, depicted in Fig. 1, is for the "Light Shining through a Wall" (LSW) experiment meant to search for photon oscillations to and from axions – a particle theorized to exist beyond the Standard Model.

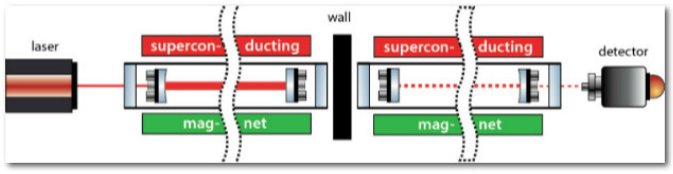

Figure 1. ALPS IIc design for axion detection.[11] The magnetic field of the production cavity is theorized to produce axions while the regeneration cavity uses the field to generate photons back from axions with a wall separating the two to prevent scattered light from reaching the detector.

A modified version of the ALPS IIc design, shown in Fig. 2, could be used for a VMB experiment. This design has an optical path of approximately 176 m that will be surrounded by 5.3 T HERA dipole magnets making the expected VMB $\Delta n = 1.1 \times 10^{-22}$ and expected path length difference $\Delta l = L\Delta n = 2 \times 10^{-20}$ m. Using infrared lasers with a wavelength of 1064 nm, this translates to a phase difference of $\Delta\varphi = 1.16 \times 10^{-13}$ rad.

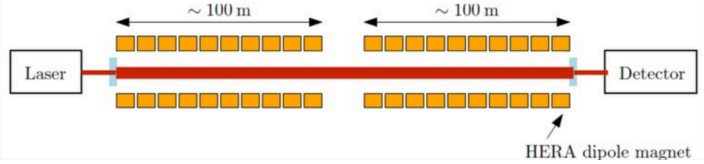

Figure 2. Modified ALPS IIc design for vacuum birefringence detection.[12] The production and regeneration cavities from the LSW experiment are combined to form a single cavity that would produce the largest single pass phase shift of any VMB experiment.

Detecting such a miniscule effect requires an immensely accurate experiment that is precisely calibrated. One aspect of this calibration is to account for the BF of external sources that could interfere with the final measurement. The illustration in Fig. 2 is simple but it can be seen that the mirrors are one of these sources so their BF must be known. Our experiment tests a new laser heterodyne polarimetry design that will be similar to the final sensing schematic by measuring the BF of mirrors.

APPARATUS

Our laser heterodyne polarimeter, as seen in Fig. 3, consists of two primary components: a path for laser locking, and a path for signal detection.

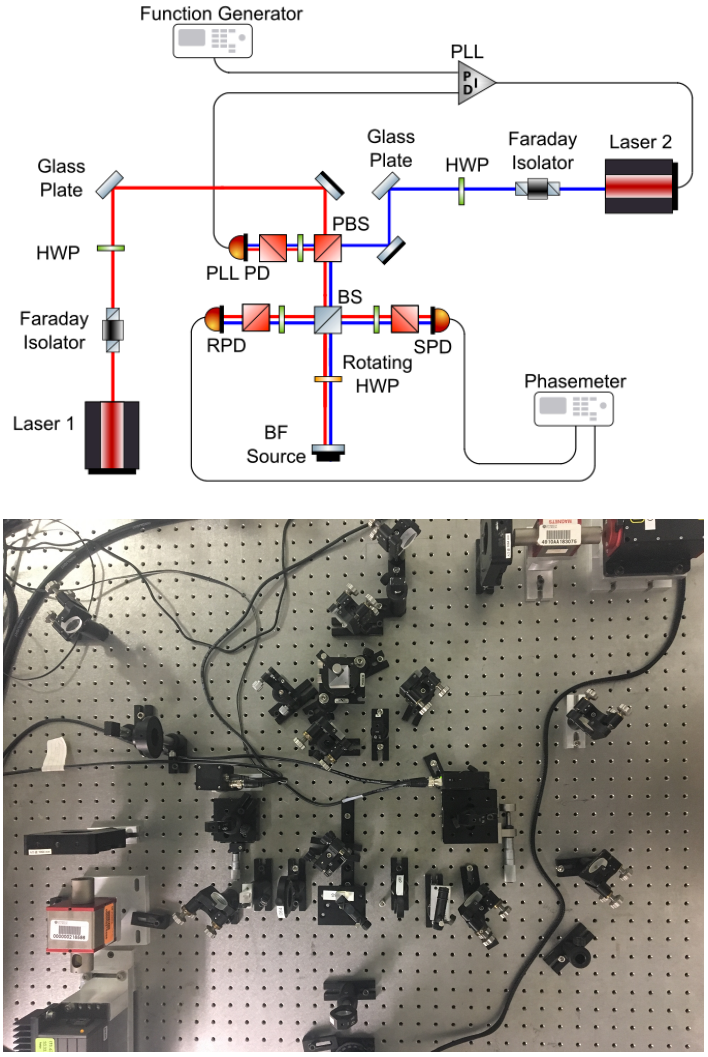

Figure 3. *Top:* LHP schematic used to measure mirror BF (BF source). From their emission, the lasers are prepared to be polarized, which occurs at the first PBS. They then travel coherently on two paths: one to the PLL PD for laser locking, and another to the BS for signal detection where they are split once more.
Bottom: View of our LHP experimental apparatus from above. The PLL PD is out of range but is located above the upper left corner.

Laser Locking

Heterodyne interferometry uses the offset frequency (beat note) between two independent lasers as a tool for various measurements. While each of our lasers operate at 1064 nm, sub-picometer fluctuations create a beat note in the megahertz. In order to obtain accurate results, this beat note must stabilized so any measurement deviations can

confidently be attributed to the source being measured. One method of stabilization is by locking the two lasers so their offset frequency and phase remain constant.

Beam Path. Each beam in our apparatus traveled through an identical set of components before being superimposed beginning with a Faraday isolator to prevent backscattered light from damaging the laser. The beams then traveled through a half-wave plate (HWP), which rotated the polarization of the incident light. One field then had p-polarized light, represented by the red line, while the other had s-polarized light, represented by the blue line. The glass plates reduced the power of each laser by one order of magnitude leaving the beams with a power of approximately 10 mW. They were then guided by steering mirrors into the first polarizing beam-splitter (PBS) where they overlapped and propagated coherently to the rest of the phase lock loop (PLL) path and the signal path. In order for the photodetector to detect a beat between the two orthogonally-polarized beams, they must first be projected into the same plane. A HWP set to 22.5° followed the combining PBS, which rotated the beams by 45°. With the use of another PBS, the s-polarization of each beam was selected giving the PLL PD a linearly polarized field containing equal power contributions from each laser.

Phase Lock. After the optical signal has been acquired to the PLL PD, several electronic components are used stabilize the beat note with specifications detailed in Table 1. The PD first coverts the optical signal to an electrical one that mixes with a signal of the same frequency from the function generator. Our chosen carrier frequency was 5 MHz because it was well within the bandwidth of all the components. The mixer then outputs the sum and difference frequencies of the two inputs before the low pass filter (LPF) selects the difference frequency, 0 Hz, with minimal loss.

Table 1. Laser locking electrical component specifications

	f_{LO}/f_{RF} (MHz)	f_{IF} (MHz)	LO Power
Mini-Circuits ZAD-6+ Mixer	0.003 – 100	DC – 100	+7 dBm
	Passband (MHz)	**Impedance**	-
Mini-Circuits BLP-5+ LPF	DC – 22	50 Ω	-
	Frequency Range	**Amplitude Range (Vpp)**	**Impedance**
SRS DS345 Synthesized Function Generator	1 μHz – 30.2 MHz	0.01 – 10 (@ 50 Ω)	50 Ω / 1 MΩ
	Bandwidth	**Gain**	**NEP**
EOT-3000A Amplified PD	30 kHz – 1.5 GHz	770 V/W (@ 1064 nm)	~39 nW/√Hz

This signal is then fed into an analog PLL made in-house that returns two outputs to minimize the drift of the beat between the two lasers. One channel outputs a "slow" correction signal to the temperature control of Laser 2 in Fig. 4. This signal is used to offset the slight drift in room temperature over hours. The second channel outputs a "fast" correction signal that can quickly adjust the voltage across the piezo crystal in the laser to offset random phase fluctuations. With these controls in place, the beat between the two lasers remains in phase with the local oscillator. From the stability of the function generator, we know the frequency of the beat is also locked.

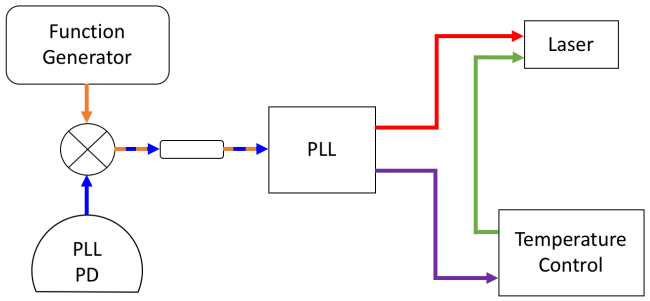

Figure 4. Laser locking electronics schematic. Signals from the PLL PD and function generator are combined in a mixer. A low pass filter selects the difference frequency to input into the PLL. One feedback loop connects directly to the piezo crystal in the laser while the other adjusts the laser's temperature control.

Signal Detection

Beam Path. Once the two beams combined at the first PBS, one path was used for locking while the other path was for signal detection. The subsequent procedure follows that of Hollis et. al.[13] The two orthogonally-polarized, phase-locked beams at this stage, shown in Fig. 3, can be represented through the Jones matrices as

$$\tilde{\mathbf{E}} = \begin{pmatrix}1\\0\end{pmatrix} A_p e^{i\omega t} + \begin{pmatrix}0\\1\end{pmatrix} A_s e^{i(\omega+\Omega)t} \qquad (4)$$

where A_p and A_s are real amplitudes and Ω is the carrier frequency. The reflected field from a beam splitter (BS) that further divides the experiment into reference and signal paths is then

$$\tilde{\mathbf{E}}_{\mathrm{R}} = \frac{1}{\sqrt{2}}\left(\begin{pmatrix}1\\0\end{pmatrix} A_p + \begin{pmatrix}0\\1\end{pmatrix} A_s e^{i\Omega t}\right) e^{i\omega t} \quad . \qquad (5)$$

The reference path simply projected the field into a single plane, as with the locking path, so a PBS selected the s-polarization after the field traveled through a HWP rotated at 22.5°. The field on the reference detector, RPD, after this combination of components is given by

$$\begin{aligned}\tilde{\mathbf{E}}_{\mathrm{RPD}} &= \begin{pmatrix}0 & 0\\ 0 & 1\end{pmatrix}\frac{1}{\sqrt{2}}\begin{pmatrix}1 & 1\\ 1 & -1\end{pmatrix}\tilde{\mathbf{E}}_{\mathrm{R}}\\ &= \frac{1}{2}\begin{pmatrix}0 & 0\\ 1 & -1\end{pmatrix}\left(\begin{pmatrix}1\\ 0\end{pmatrix}A_p + \begin{pmatrix}0\\ 1\end{pmatrix}A_s e^{i\Omega t}\right)e^{i\omega t}\\ &= \frac{1}{2}\begin{pmatrix}0\\ 1\end{pmatrix}\left(A_p - A_s e^{i\Omega t}\right)e^{i\omega t} \quad . \end{aligned} \tag{6}$$

It follows that the intensity is

$$I_{\mathrm{RPD}} = \left|\tilde{\mathbf{E}}_{\mathrm{RPD}}\right|^2 = \frac{1}{4}\left(A_p^2 + A_s^2\right) - \frac{1}{2}A_p A_s \cos\Omega t \quad . \tag{7}$$

The RPD signal was used as a standard measurement for noise inherent to the setup. Since we only desired to detect the BF from the source mirror, a BB1-E03 Broadband Dielectric mirror from Thorlabs, any extraneous effects could be eliminated by subtracting the phase information on RPD.

The signal path began with the BS transmission field:

$$\tilde{\mathbf{E}}_{\mathrm{T}} = \frac{i}{\sqrt{2}}\left(\begin{pmatrix}1\\ 0\end{pmatrix}A_p + \begin{pmatrix}0\\ 1\end{pmatrix}A_s e^{i\Omega t}\right)e^{i\omega t} \quad . \tag{8}$$

The field propagated through another HWP but now one rotated at an angle θ_π before reflecting off the source mirror rotated at θ_m. The phase of each polarization after this reflection is denoted ϕ_x and ϕ_y. The field, after propagating back through the rotated HWP, is then represented:

$$\begin{aligned}\tilde{\mathbf{E}}_{\mathrm{T}} = \frac{i}{2\sqrt{2}}\Bigg\{&\begin{pmatrix}2e^{i\phi_x}\cos 2\gamma\\ \left(e^{i\phi_x} - e^{i\phi_y}\right)\sin 2\gamma\end{pmatrix}A_p\\ &+\begin{pmatrix}\left(e^{i\phi_x} - e^{i\phi_y}\right)\sin 2\gamma\\ 2e^{i\phi_y}\cos 2\gamma\end{pmatrix}A_s e^{i\Omega t}\Bigg\}e^{i\omega t}\end{aligned} \tag{9}$$

where $\gamma = 2\theta_\pi - \theta_m$. Finally, the field is reflected at the BS and enters an equivalent HWP-PBS combination as before all PDs. This field, represented by

$$\begin{aligned}\tilde{\mathbf{E}}_{\mathrm{SPD}} = \frac{i}{4\sqrt{2}}\Big\{&\left(e^{i\phi_x} - e^{i\phi_y}\right)\left(A_p + A_s e^{i\Omega t}\right)\cos 2\gamma\\ &-\left(e^{i\phi_x} - e^{i\phi_y}\right)\left(A_p - A_s e^{i\Omega t}\right)\sin 2\gamma\\ &+\left(e^{i\phi_x} + e^{i\phi_y}\right)\left(A_p - A_s e^{i\Omega t}\right)\Big\}e^{i\omega t}\end{aligned} \tag{10}$$

now contains a phase-shifted beat note compared to the RPD signal because of the mirror's BF. In the case when this BF, $\delta \equiv \phi_x - \phi_y$, is small, we can approximate the intensity on the signal PD to be

$$\begin{aligned}I_{\mathrm{SPD}} &\approx \frac{1}{8}\left(A_p^2 + A_s^2\right) - \frac{1}{4}A_p A_s(\delta\cos 2\gamma \sin\Omega t + \cos\Omega t)\\ &\approx \frac{1}{8}\left(A_p^2 + A_s^2\right) - \frac{1}{4}A_p A_s\cos(\Omega t + \phi)\end{aligned} \tag{11}$$

where $\phi = 2\delta\cos 2\gamma = 2\delta\cos(4\theta_\pi - 2\theta_m)$. By rotating the HWP at a constant angular velocity such that $\theta_\pi = \omega_\pi t$, we show that

$$\phi = \delta\cos(4\omega_\pi t - 2\theta_m) \quad . \tag{12}$$

Thus, with ideal components, the mirror's BF produces a signal at four times the rotation rate of the HWP with amplitude δ.

We were able to rotate the HWP consistently using a set of Thorlabs components: a DDR05 rotation mount, a KBD101 K-Cube Brushless DC Servo controller, and an APT system software. The physical rotation of the mirror was possible due to the mount, which was controlled by a brushless motor capable of steps, jogs, and continuous rotation. The motor's actions were then controlled by the APT software where the rotation rate was set to 5 Hz.

With imperfect components, Eq. 12 deviates slightly. An error in the rotating HWP can be modeled by adjusting its retardation to $\pi + \epsilon$. Taking only first order terms in δ and ϵ, an extra factor of

$$\frac{\epsilon}{2}A_p A_s \cos 2\theta_\pi \sin\Omega t \tag{13}$$

arises in the SPD intensity when again considering δ to be small. Letting $\theta_\pi = \omega_\pi t$ in Eq. 13, Eq. 12 then becomes

$$\phi = \delta\cos(4\omega_\pi t - 2\theta_m) - 2\epsilon\cos 2\omega_\pi t \tag{14}$$

showing a signal from the HWP error appears at twice its rotation rate with an amplitude of 2ϵ.

In order to ensure the mirror's BF signal does not appear at a frequency laced with other spurious signals, we extended the SPD intensity to include the next higher order term in ϵ:

$$-\frac{\epsilon^2}{4}A_p A_s(1 + \cos 4\theta_\pi)\cos\Omega t \quad . \tag{15}$$

This leads to a beat note phase shift of

$$\phi \approx \delta\cos(4\omega_\pi t - 2\theta_m) - 2\epsilon\cos 2\omega_\pi t - \frac{\epsilon^3}{3}\cos 6\omega_\pi t \,, \tag{16}$$

which identifies an additional peak at six times the HWP rotation due to its retardation error, but no additional signal at $4\omega_\pi t$ – the frequency of the mirror BF signal.

Phase Processing. To gather phase information from the RPD and SPD, we used a Moku:Lab Phasemeter[14] from Liquid Instruments. This instrument tracked the phase, frequency, and amplitude of each PD through two independent channels. The interface was provided through an iPad application, seen in Fig. 5, and provided optimal control of various parameters.

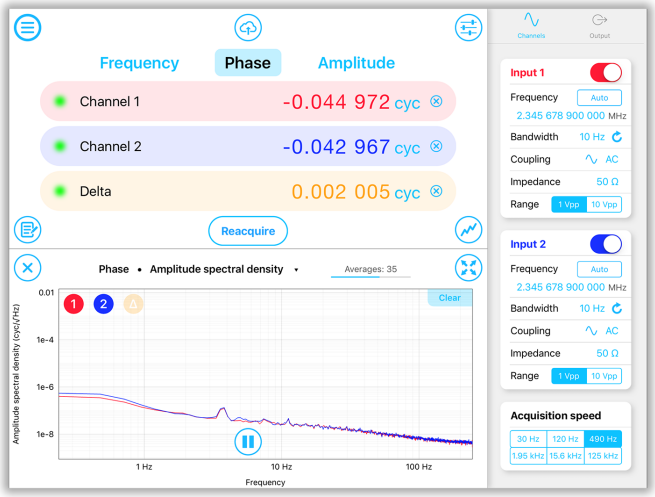

Figure 5. Moku:Lab Phasemeter iPad interface. Input 1 and 2 had the same settings: 5 MHz reference frequency, 10 kHz bandwidth, AC coupling, 50 Ω impedance, and a range of 1 Vpp.

Each channel locked onto a reference frequency equal to that of our beat note with a 1 Vpp range since the maximum RPD and SPD voltages were approximately 0.6 V and 0.3 V respectively. The sampling rate was set to the 120 samples per second (S/s) setting although the true value was closer to 122.07 S/s. Data was saved as a CSV file which was then used for analysis in MATLAB. To convert the raw phase data into plots containing the amplitudes of various BF signals, we took the discrete Fourier transform (DFT) of the phase difference between the two channels.

SPATIAL VARIANCE

One test performed on the mirror involved determining how its BF varied when probed at different locations on its surface.

Procedure

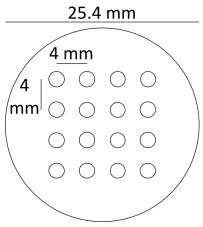

Figure 6. Actual-size image of mirror with 4 x 4 spatial grid of beam locations. To ensure the beam was not clipped, we approximated it to be contained within a 2 mm diameter circle at the mirror's surface.

In order to obtain a BF surface map, we needed to be able to adjust the mirror's position in the 2-D plane perpendicular to the incident light. We used a combination of a Thorlabs 6XS mirror mount and a Newport 460-XYZ mount to accomplish this with enough translational freedom to cover a significant portion of the mirror's surface. We then constructed a 4 x 4 grid of points, shown in Fig. 6, to effectively probe 144 mm^2, which maximized our area covered while maintaining that the beam was fully reflected. A two-minute measurement was taken at each point.

Results and Conclusions

It is shown from Fig. 7 that the birefringence across the mirror's surface varied approximately 2 mrad from 22.4 to 24.4 mrad. In comparison, repeated measurements on a single point showed a standard deviation of approximately 0.2 mrad. Both plots showed the maximum BF at the point second from the bottom and left while the minimum BF was at the point directly above it.

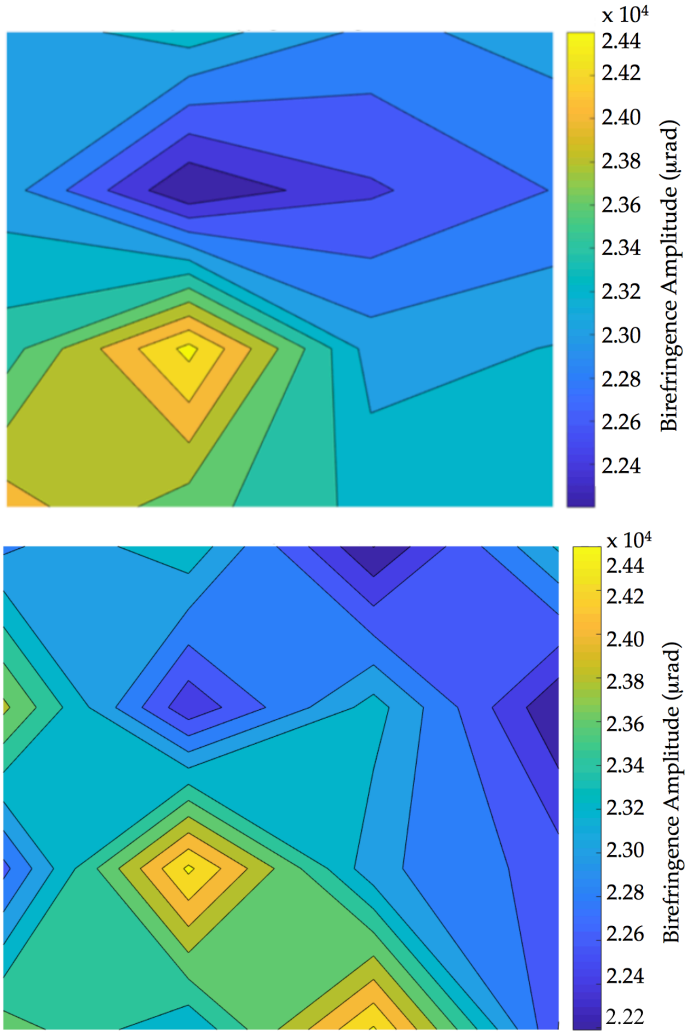

Figure 7. Interpolated plots of spatial BF variance. Over multiple runs, the mirror's total BF variance and average BF remained constant at 2 mrad and 23 mrad respectively. The gradients were created through MATLAB.

These values were consistent over multiple runs covering all 16 points before measuring another point again. The surface fluctuations can therefore be attributed to imperfections over random error. Since this mirror, a BB1-E03 Broadband Dielectric mirror from Thorlabs, is composed of a polished glass substrate under alternating

layers of reflective coatings, we can conclude the imperfections are due to errors in the coating layers.

MAGNETIC EFFECTS

The 5 T magnets present in the modified ALPS IIc design from Fig. 2 will produce strong fields outside of their intended target area. The mirrors will therefore be subject to some amount of these stray fields. In order to precisely characterize all BF effects and eliminate the possibility of a false positive when attempting to detect VMB, we examined how a mirror's BF varied when placed in a magnetic field parallel to its surface.

Apparatus and Procedure

First, we wanted to ensure all measurements contained contributions strictly from the magnetic effect so we inserted a telescope between the rotating HWP and source mirror. This expanded the beam so its cross-sectional area at the mirror was nearly as large as the mirror's surface itself. With this beam expander in place, the minor surface variations were averaged out giving us a more stable measurement for the mirror's BF on its own.

To replicate the stray fields present on the mirror's surface, we obtained strong magnets and created a device to hold them in place over a range of distances. The four magnets we used were 2" x 1" x 3/8" N52-Neodynium magnets (BY0X06-N52) from K&J Magnets, Inc. that each produced a surface field strength near the 3400 Gauss advertised. We were able to measure this with a Gauss meter and calculate it using the following equation provided by K&J Magnets, Inc.:

$$B = \frac{B_r}{\pi}\tan^{-1}\left(\frac{LW}{2z\sqrt{4z^2+L^2+W^2}}\right) - \tan^{-1}\left(\frac{LW}{2(D+z)^2\sqrt{4(D+z)^2+L^2+W^2}}\right) . \quad (17)$$

In Eq. 17, B_r is the remanence field, L, W, and D are the length, width, and thickness of the magnet respectively, and z is the distance away from a pole assuming the poles are oriented with the axis of the thickness. The units of L, W, D, and z are arbitrary so long as they are all the same. The theoretical and measured fields for a single magnet are plotted in Fig. 8.

The holders, shown in Fig. 9, had spaces to fit each magnet independently, which would produce a combined field that is parallel to the surface of the mirror. The holders also had holes for the two poles on either side that had distance markings on them. This, in conjunction with the side screws, allowed us to adjust the distance of the magnets from the mirror in eighth-inch increments and thus alter the field strength present at the mirror's surface. In addition, the casings were made out of phenolic making neither them nor the mirror mount magnetic.

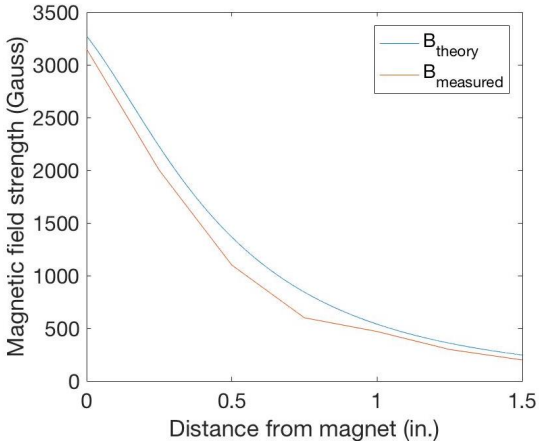

Figure 8. Plot of magnetic field strength vs distance from a magnet pole for a single N52-neodymium magnet. Neither the measured nor the theoretical calculation reach 3400 Gauss at the magnet's surface but the two curves align nonetheless.

With all four magnets in place, we took two minute measurements at eighth-inch increments. The nearest position is depicted in Fig. 9 and is when the closest magnet is one inch from the center of the mirror. The furthest position is when the bottom casing is sitting on the table, which makes the closest magnet 2.5 inches from the mirror's center.

Results and Conclusions

As seen in Fig. 10, the BF of a New Focus 5104 mirror remains essentially unchanged over a range of nearly 1000 Gauss. The uncertainty in field strength arises from the sixteenth-inch uncertainty in our distance measurements while the uncertainty in our BF amplitude was determined after repeated measurements. The mean BF amplitude was 18,200$\pm$400 μrad, which was near the initial value and on the final value even in a magnetic field great than 1 kG.

Figure 9. Lab photograph of magnet holder surrounding the mirror. Rulers at the poles allowed us to vary the distance in eighth-inch increments. The casings themselves were crafted out of a non-magnetic material named phenolic.

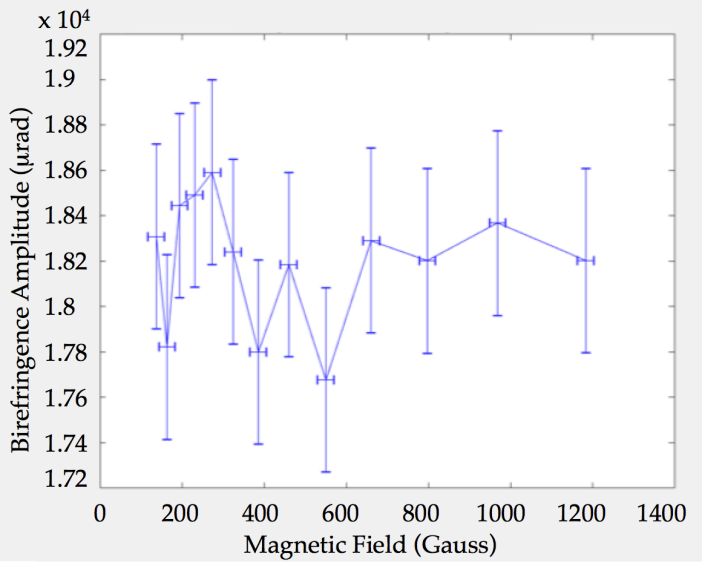

Figure 10. Plot of BF vs magnetic field strength for the New Focus 5104 mirror. No correlation between BF and field strength can be determined with our error for field strengths in this range.

SIGNAL ISOLATION

From Eq. 14, we expect BF signals at twice and four time the rotation rate of the HWP and from Eq. 16, we can even expect a small signal at six times this rate. When observing the DFT of the phase difference between our two channels, however, we spot these peaks along with others at integer multiples of the rotation rate, as seen in Fig. 11.

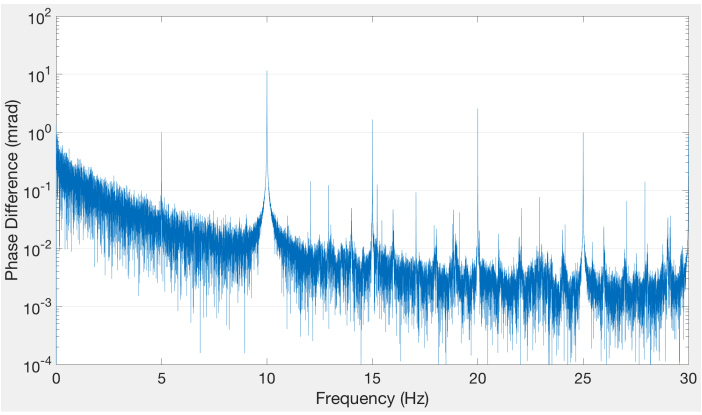

Figure 11. Phase difference DFT showing strong peaks at 10 and 20 Hz from the HWP error and mirror respectively. The origin of other significant peaks at higher harmonics of 5 Hz are being investigates.

In an attempt to confirm the 20 Hz amplitude as only our mirror's birefringence, we utilize the notion that under constant rotation, we can set $\theta_m = \omega_m t$ so Eq. 14 becomes

$$\phi = \delta\cos(4\omega_\pi t - 2\omega_m t) - 2\epsilon\cos 2\omega_\pi t \qquad (18)$$

meaning the mirror's BF signal can be moved off 20 Hz. We used a function generator connected to a stepper motor that controlled the gears on a mirror mount to set the mirror's rotation rate to 3.5 Hz in the opposite direction of the HWP rotation.

Results and Conclusions

According to Eq. 18, the mirror's birefringence should have moved to 27 Hz with an amplitude of δ and that is exactly what we see, shown in Fig. 12.

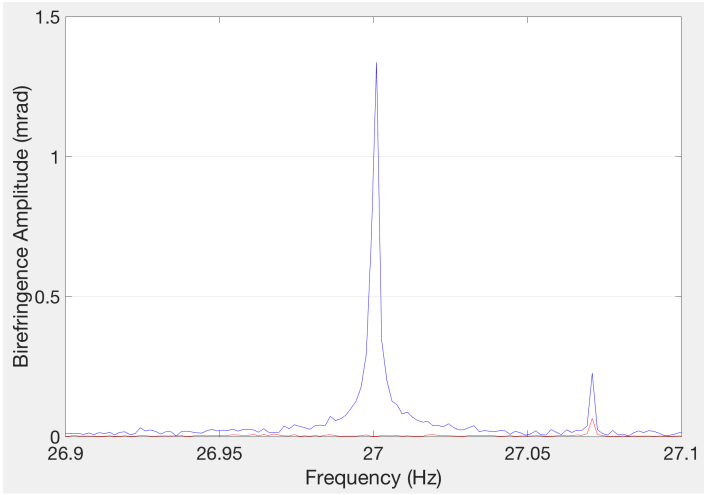

Figure 12. Isolated mirror BF signal. The red line represents the signal BF when only the HWP is rotating (5 Hz) while the blue line represents the signal BF when both the HWP and mirror are rotating (5 Hz, 3.5 Hz).

The BB1-E03 mirror's BF was determined to be 1.34 mrad with phase noise of 2 μrad/√Hz. From this, we can reach a sensitivity of 0.1 μrad in 400 s averaging time, matching the precision of previous experiments[15] without the complications of a cavity.

Unfortunately, including the mirror's own rotation rate introduced peaks at its fundamental frequency and higher harmonics, as seen in Fig. 13. We know that a signal will appear at the mirror's rotation rate if the rotation axis is not perfectly aligned with the incident beam but are unclear about the other peaks.

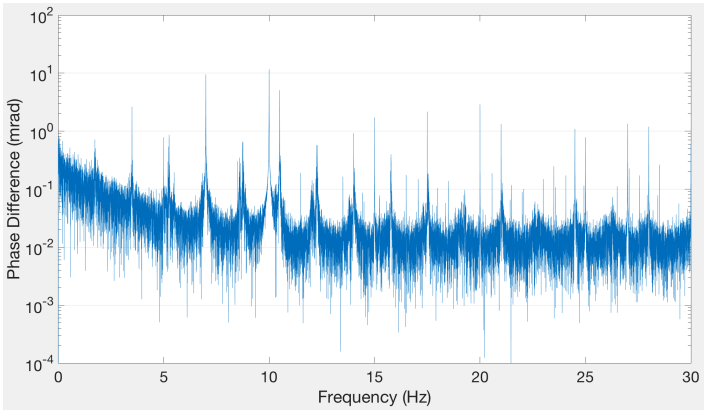

Figure 13. DFT spectrum with both the mirror rotating at 3.5 Hz and the HWP rotating at 5 Hz. The 10 Hz and 20 Hz amplitudes are nearly equal to what they were in Fig. 11 but surround by more noise from the combined harmonics of the mirror's and HWP's rotation.

OUTLOOK

While we were able to successfully measure the mirror's birefringence at an independent frequency with no other BF contributions, we would like to eliminate the excess noise and higher harmonics to create a more sensitive experiment for VMB detection. The magnets in ALPS IIc will have the capability of fluctuating between 50% and 100% power at a slow rate (~1 mHz), which would produce sidebands around the HWP rotation frequency. The sidebands would also be at a frequency uncorrupted by excess rotation noise. We can simulate this procedure by keeping the mirror at a fixed angle and inputting an electro-optic amplitude modulator (EOAM) after the rotating HWP and before the source mirror. Early findings show promise that even a weak signal from sending a 0.01 Vpp sin wave at 1 Hz to the EOAM can be distinguished with a BF of 400 μrad.

ACKNOWLEDGMENTS

I would first like to thank Guido Mueller for giving me the opportunity to work on this project two years ago. I would also like to thank Hal Hollis for helping me understand the fundamentals of this experiment, Harrison LaBollita for his contributions to the experiment over last summer, and Claire Baum for constructing the foundations of the experiment two summers ago. Finally, I would like to thank my family for their love and support even without knowing what I really work on and my girlfriend, Hannah, for always encouraging me during the entire writing process and beyond.

This material is based upon work supported by the Heising-Simons Foundation under Grant No. 0009872.

REFERENCES

[1]P. A. M. Dirac, Proc. Cambridge Philos. Soc. **30** (2), 150-163 (1934)

[2]W. Heisenberg, Zeit. Phys. **90**, 209-231 (1934)

[3]Robert Serber, Phys. Rev. **48**, 49-54 (1935)

[4]E. A. Uehling, Phys. Rev. **48**, 55-63 (1935)

[5]W. Heisenberg, H. Euler, Zeit. Phys. **98**, 714-732 (1936)

[6]Robert Karplus and Maurice Neuman, Phys. Rev. **80**, 380-385 (1950)

[7]E. Iacopini, B. Smith, G. Stefanini, E. Zavattini, Nuovo Cimento B **61**, 21-37 (1981)

[8]R. Cameron et. al., Phys. Rev. D **47**, 3707-3725 (1993)

[9]E. Zavattini et al. (PVLAS Collaboration), Phys. Rev. D **77**, 032006 (2008)

[10]John L. Hall, Jun Ye, and Long-Sheng Ma, Phys. Rev. A **62**, 013815 (2000)

[11]ALPS, Present and Future of ALPS II, https://alps.desy.de/e191931/

[12]G. Mueller et al., in APS April Meeting 2016 **61**, Available online at: http://meetings.aps.org/link/BAPS.2016.APR.U16.4 (2016)

[13]Harold Hollis, Gabriel Alberts, David Tanner, Guido Mueller, arXiv:1710.03801v1 [physics.ins-det] (2017)

[14]Moku:Phasemeter, http://www.liquidinstruments.com/phasemeter/

[15]A. J. Fleisher, D. A. Long, Q. Liu, and J. T. Hodges, Phys. Rev. A **93**, 1–7 (2016)